Atomic collisions with relativistic heavy ions. III. Electron capture

W. E. Meyerhof and R. Anholt
Department of Physics, Stanford University, Stanford, California 94305-2196

J. Eichler*
Molecular Physics Department, SRI International, Menlo Park, California 94025
and Department of Physics, Stanford University, Stanford, California 94305-2196

H. Gould and Ch. Munger
Materials and Molecular Research Division, Lawrence Berkeley Laboratory, University of California, Berkeley, California 94720

J. Alonso
Accelerator and Fusion Research Division, Lawrence Berkeley Laboratory, University of California, Berkeley, California 94720

P. Thieberger and H. E. Wegner
Department of Physics, Brookhaven National Laboratory, Upton, New York 11973
(Received 30 July 1985)

Cross sections for the electron capture by 82- , 140- , and 200-MeV/amu Xe^{54+}, Xe^{53+}, and Xe^{52+} ions incident on thin solid targets from Be to Au were measured. The measurements are compared with calculations of radiative and nonradiative capture. The nonradiative capture calculations are based on the relativistic eikonal approximation which includes transitions from K, L, and M shells of the target to nearly all projectile shells. In high-Z targets, nonradiative capture into excited states of the projectile is dominant, as predicted by the eikonal calculations and confirmed by comparing measured cross sections for bare Xe^{54+} and Xe^{52+} ($1s^2$) projectiles. A simple formula for estimating nonradiative-electron-capture cross sections for relativistic-ion accelerator design and other applications is derived. Double and triple electron capture are also observed in the low-velocity, high-Z collisions.

I. INTRODUCTION

The critical step in understanding collisional processes affecting relativistic heavy ions in matter is the formulation and verification of a theory of nonradiative electron capture (NRC).[1] Several measurements of electron capture by relativistic low-Z (C, Ne, and Ar ions)[2] and by Au and U ions[3,4] have been reported recently. The low-Z measurements relied heavily on theoretical calculations of stripping and excitation cross sections to obtain electron-capture cross sections from equilibrium charge states;[1] hence they are only indirect determinations. In the measurements with U ions, thick targets were used and the capture cross sections were obtained from a least-squares fit of the charge-state dependence on target thickness.[5] In the present work, we have obtained an accurate determination of electron capture and stripping cross sections by measuring the yields for the pickup and stripping of one or two electrons from zero-, and one-, or two-electron ions in thin targets.

A precise knowledge of electron capture and stripping cross sections at relativistic velocities has several important applications. Gould *et al.*[3] and Thieberger *et al.*[4] have stressed the application of such studies to energy-loss measurements and relativistic-ion accelerator design. The electron capture and stripping cross sections determine the ability of stripping foils to provide high yields of nearly bare projectiles and the lifetime of circulating heavy ions in storage rings or synchrotrons due to charge-changing collisions. The energy loss of heavy ions in foils and Z identification in ΔE detectors depend on the projectile charge state, which can be determined from a knowledge of electron capture and stripping cross sections.

One of the aims of the present series of papers is the development of a complete theory of relativistic ions in matter, including electron capture into ground and excited states and the ionization of ground state and excited electrons in few-electron projectiles. This theory requires precise experimental information and an accurate theory of electron capture, capable of predicting fine details like cross sections from state to state.

For relativistic heavy ions, only three quantitative theories of NRC are presently available. The relativistic Oppenheimer-Brinkmann-Kramers (OBK) theory of Shakeshaft[6] and Moiseiwitsch and Stockman[7] predict cross sections for low-Z projectiles that are more than a factor of 3 too high compared with experiment.[1] This is typical of results seen also at nonrelativistic velocities where the application of second-Born-approximation theories improve the agreement between theory and exper-

iment.[8] For low-Z relativistic heavy ions, even second-Born-approximation calculations[9] are generally higher than experiment.[10,11]

In the present work, the measured cross sections are compared with eikonal approximation calculations.[11,12] The eikonal approximation is a high-energy approximation, which was found to give good agreement with experiment for low-Z ions if the ion velocity (in atomic units) exceeds approximately $2Z_T$, where Z_T is the target atomic number (in this case, the higher of the projectile or target atomic numbers).[11] For low-Z ions, capture of target K electrons into the projectile K shell is the dominant contribution to the total capture cross sections. We find that for high-Z ions and targets, the cross sections for the capture of target L and M electrons into the projectile K, L, and M shells are all of comparable magnitudes to the K to K cross sections at lower velocities. The present eikonal calculations include the target K, L, and M shells and all projectile shells up to $n=10$.

Section II of this paper describes measurements of electron capture and ionization cross sections by magnetic charge-state dispersion techniques. In Sec. III A, the eikonal approximation[12] is applied to calculate state-to-state electron-capture transitions for each projectile and target shell. One of the formal difficulties with the eikonal approximation is that it is an asymmetric theory. One active-electron-nucleus interaction is treated in higher-order and the other interaction is treated in first-order perturbation theory. Depending on which interaction is chosen, different cross-section results are obtained. This post-prior discrepancy is examined in Sec. III B, where a prescription is proposed for deciding which choice to make. Comparison with the present experimental results is made in light of this prescription. Because of the great success of the present numerical eikonal calculations, but their inherent complexity, we developed a simple formula based on scaling considerations for NRC cross sections for capture from any target shell to any projectile shell from an approximate formula for K to K transitions.[12] This formula is discussed in Sec. III C, and is useful for estimating capture cross sections, such as might be needed for accelerator design and energy-loss measurements.[4] Radiative electron capture (REC) into higher projectile shells is discussed in Sec. III D. Results and comparison with the *ab initio* theory as well as the scaling formulas are given in Sec. IV.

II. EXPERIMENT

A. Experimental apparatus

Xe beams from the Lawrence Berkeley Laboratory's Bevalac were used. The experimental arrangement is shown in Fig. 1. Upstream of the "target area," and in front of bending magnets not shown in the figure, 50—250-μm Mylar foils were inserted into the beam. The foil thicknesses were chosen to optimize the intensity of the charge-state selected, incident Xe^{54+}, Xe^{53+}, or Xe^{52+} beams at the particular incident energy, 85-, 140-, or 200-MeV/amu. The stripping foils were thick enough to reduce the 85-MeV/amu Xe beam by 3.5 MeV/amu and the 200-MeV/amu Xe beam by 1 MeV/amu, hence the beam energies are uncertain by about 1—3.5 MeV/amu. This has a negligible effect on the projectile ionization cross sections, and at most a 20% effect on the capture cross sections. In the target box, a set of 50 Be, Mylar (abbreviated My below), Al, Cu, Ag, and Au foils was available which could be remotely inserted into the beam. The target frames were 1.6-mm-thick Al disks with 1.9—3.8-cm-diam center holes. The thinnest Cu, Ag, and Au targets ($\leq$0.1 mg/cm^2) were mounted on 0.05-mg/cm^2 C backings; thicker foils were self-supporting.

After passing the primary beam through the foils, the charge states were separated by a magnetic spectrometer, originally designed to study projectile nuclear fragmentation by Greiner *et al.*[13] and first used for electron-capture measurements by Crawford.[2] Approximately 7-m downstream from the target box, the charge states were focused by a set of quadrupole magnets (B40Q2A and B40Q2B in Fig. 1), and were dispersed by two dipole magnets (B40M2 and M3) into a large vacuum chamber. The exit window on the vacuum chamber caused only negligible scattering of the charge-state beams, which then entered a position-sensitive proportional counter. This $\sim$50-cm-long detector could be rolled along the exit window of the chamber.

At any given detector location, up to ten charge states could be detected simultaneously. The most critical and time consuming part of the experiment consisted of minimizing the quadrupole steering in the vertical direction which if present would result in different vertical positions of the charge-state peaks at the detector, different detection efficiencies, and degraded detector resolution. For this purpose, Polaroid film was placed on the en-

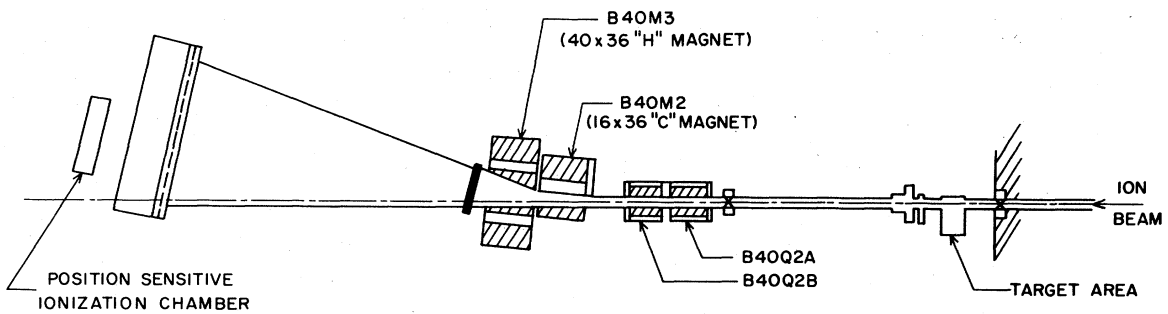

FIG. 1. Schematic diagram of the experimental apparatus. Target foils were inserted into the beam in the box marked "target area." The magnets B40Q2A and Q2B were quadrupole, and B40M2 and M3 dipole. The dipole magnets dispersed the charge-state beams into a large vacuum chamber. The position-sensitive detector could be rolled along the exit window of the vacuum chamber.

trance window of the position-sensitive detector, and the beam focusing was adjusted until satisfactory charge-state beam spots were obtained on the film. The charge-state spectrum was then swept magnetically across the detector to assure a uniform detection efficiency of the detector along its entire front face. This procedure had not been followed in earlier experiments with this apparatus,[3,4] suggesting the possibility of considerable systematic error. The relative errors would be largest in the ratios of widely separated charge states, and least in adjacent ones. Measured cross sections for uranium beams[3] quote a factor of 2 uncertainty, which is large enough to accommodate systematic errors.

Figure 2 shows a pulse-height spectrum in the detector for 200-MeV/amu Xe^{53+} passing through 10-mg/cm^2 Be. Besides the unaltered Xe^{53+} peak, a Xe^{54+} peak representing one-electron loss (projectile K-shell ionization), and a Xe^{52+} peak representing one-electron attachment (capture into vacant projectile states from all filled target states) are observed. With thicker or higher-Z targets, more charge states were seen.

B. Data analysis

In essence, two methods, called here "thin target"[14] and "thick target,"[15] exist for extracting charge-changing cross sections from a measurement of charge-state yields as a function of target thickness. In the thin-target method, targets are chosen that are thin enough so that the yield for one-electron attachment or loss is proportional to the target thickness. The charge-changing cross sections can then be obtained very simply from the proportionality factors. In the thick-target method, the target thickness is varied up to the equilibrium thickness.

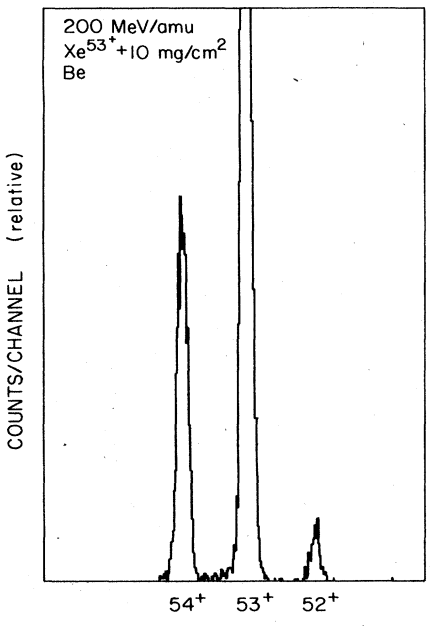

FIG. 2. Pulse-height spectrum from the position-sensitive detector for 200-MeV/amu Xe^{53+} traversing 10-mg/cm^2 Be. The spatial separation between adjacent charge-state peaks was approximately 1.9 cm.

Charge-changing cross sections are obtained by a least-squares fit of the data to the integrated rate equations for charge-state yields.[5,15]

The advantage of the thin-target method, used here, is its simplicity and lack of ambiguity in extracting charge-changing cross sections. The disadvantage is that low counting rates are obtained for the charge-changing yields. Hence, even small backgrounds from scattering on slits or target frames could prevent an accurate determination of peak areas (Fig. 2). For this reason, we also took data with thick targets, which will be presented in a later paper in this series.

Integration of the charge-changing rate equation[15] is very simple if the yield is proportional to the target thickness. In general, we assume that a beam initially containing fractions F_0, F_1, and F_2 of zero-, one- and two-electron ions traverses a foil containing T atoms per unit area. Then the fractions Y_n of ions bearing n electrons are given by

$$Y_0=F_0+[-F_0(a_0+h_0+g_0)+F_1s_1+F_2d_2]T+O(T^2)\,, \tag{1a}$$

$$Y_1=F_1+[F_0a_0-F_1(a_1+h_1+g_1+s_1)+F_2s_2]T+O(T^2)\,, \tag{1b}$$

$$Y_2=F_2+[F_0h_0+F_1a_1-F_2(a_2+h_2+g_2+s_2+d_2)]T+O(T^2)\,, \tag{1c}$$

$$Y_3=(F_0g_0+F_1h_1+F_2a_2)T+O(T^2)\,, \tag{1d}$$

$$Y_4=(F_1g_1+F_2h_2)T+O(T^2)\,, \tag{1e}$$

$$Y_5=F_2g_2T+O(T^2)\,. \tag{1f}$$

In these equations a_n, h_n, and g_n represent one-, two-, and three-electron attachment cross sections, respectively, for an n-electron ion; s_n and d_n represent one- and two-electron stripping cross sections, respectively, for an n-electron ion. The symbol $O(T^2)$ represents terms of order T^2 and higher powers of T which differ for the different charge fractions. We did not find evidence for any other multiple charge-changing cross sections. The lowest fraction Y_n measured was 10^{-3}. With a pure incident-charge state, e.g., $n=1$, one sets $F_1=1$, and $F_0=F_2=0$ in the above equations. One then obtains simple expressions for the charge-changing cross sections in the limit of infinitesimal target thickness T, $s_1=Y_0/T$, $a_1=Y_2/T$, $h_1=Y_3/T$, and $g_1=Y_4/T$ in this example. If the targets were mounted on a backing foil facing the beam, the appropriate values of the F's were determined from measurements with a backing foil (0.05-mg/cm^2 C). None of the charge-changed F's from the backing foil were greater than 0.005, which necessitated only small corrections except in the case of the thinnest, backed targets ($\leq$0.01-mg/cm^2 Cu, Ag, and Au).

Only in a few cases were the targets thin enough to give ratios Y_n/T that were independent of T. Figure 3 illustrates this for Xe^{53+} + Be charge-changed yields. The Y_n/T data points were least-squares fitted to straight lines to obtain the $T=0$ intercept.

For multiple charge-changing cross sections, the terms

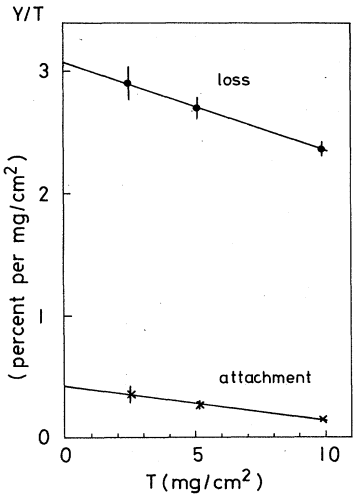

FIG. 3. Dependence of the yield to target thickness ratio Y/T on target thickness T for 200-MeV/amu Xe^{53+} traversing Be. One-electron loss is shown by closed circles and one-electron attachment by crosses. Cross sections were obtained from the $T=0$ intercept.

of order of T^2 are partly due to sequential single charge-changing processes. One could then try to correct the measured multiple charge-changing yields for these sequential processes in an attempt to reduce the terms of order of T^2. Unfortunately, it is not possible to eliminate them completely. As an illustration, the case of double ionization of the two-electron beam ($F_2=1$, $F_0=F_1=0$) may be used. Integrating the rate equations to order T^2, one finds the following for this case (assuming $h_n=g_n=0$):

$$Y_0=d_2T+[s_1s_2-d_2(a_0+a_2+s_2+d_2)]T^2/2\ ,$$
$$Y_1=s_2T+O(T^2)\ . \tag{2}$$

Setting $s_2=2s_1$ (as expected since the ionization of one of two $1s$ electrons is twice as likely as ionization of one), one can express the term $s_1s_2T^2/2$ in terms of the measured yield Y_1, and finds

$$(Y_0-Y_1^2/4)/T=d_2-d_2(a_0+a_2+s_2+d_2)T/2\ . \tag{3}$$

Unfortunately, the term proportional to T is not negligible, so that the intercept at $T=0$ must be used to determine d_2. Hence, we simply fit the individual values of Y_n/T to straight lines to obtain the $T=0$ intercept.

III. THEORY

Encouraged by the agreement of exploratory calculations[11] with experimental data[1,2] we have based the present analysis of NRC entirely on the relativistic eikonal approximation.[12] This approach,[16] in its prior (post) version, treats the electron-projectile (electron-target) interaction in first order while the electron-target (electron-projectile) interaction is treated in all orders of perturbation theory, albeit in an approximate way. The conceptual basis of the eikonal approximation has been discussed in detail,[17,18] and it has been shown that, physically, the prior version of the theory describes a hard collision of the electron with the projectile nucleus followed by multiple soft collisions with the target nucleus. Similarly, the post version of the theory describes a hard collision of the electron with the target nucleus preceded by multiple soft collisions with the projectile nucleus. The approximate summation of multiple-scattering terms, characteristic of the eikonal approximation, avoids divergent terms that can arise[19] in exact perturbation summations, e.g., in the strong-potential Born approximation.[20]

A. Capture cross sections for higher initial and final shells

The relativistic eikonal theory developed in Ref. 12 expresses the capture cross section in terms of density matrices separately describing initial and final ensembles (in the following, usually called "states") of unpolarized projectiles and target atoms. The prior version of the cross section per electron initially bound with angular momentum j is given by Eq. (2.18) of Ref. 12:

$$\sigma_{fi}=\frac{(2\pi)^4}{2j+1}\frac{\eta^2}{\gamma^2}Z_p^2\int \mathrm{Tr}\,(SP_gSP_h)d^2\mathbf{p}_b\ , \tag{4}$$

where $\eta=1/v$ is the inverse of the projectile velocity, $\gamma=(1-v^2/c^2)^{-1/2}$ is the relativistic energy parameter, and Z_p (Z_t) is the projectile (target) atomic number. Atomic units are used here and below. The integration extends over the transverse momentum $\mathbf{p}_b$. The integrand is expressed as the trace of four 4×4 matrices, which are built up from blocks of simple 2×2 matrices that can be handled easily. Here S is a relativistic spinor transform and P_g and P_h (in the prior form) characterize final and initial states, respectively. It is obvious from Eq. (4) that the density-matrix formulation,[12] in contrast to the spinor formulation,[7] allows one to factor target and projectile properties into individually calculable matrices.

In Ref. 12, formulas for P_g and P_h for arbitrary initial and final states have been given and, moreover, explicit expressions of SP_gS for final relativistic $1s_{1/2}$, $2s_{1/2}$, $2p_{1/2}$, and $2p_{3/2}$ states have been derived. Detailed cross-section formulas for these transitions have also been worked out and applied to specific cases.[11]

In the following, an outline is given of how the general framework has been applied to evaluate the contribution of higher initial and final shells. Numbers of formulas refer to Ref. 12. We first note that owing to the more complicated form for P_h, Eq. (5.9), the explicit structure of the cross-section formula is determined by the initial state (in the prior form) alone, whereas the final state affects only the quantities to be inserted in SP_gS of Eq. (3.15). Therefore, since the transitions of interest are those connecting initial K, L, and M states to final K, L, M, and higher states we may proceed as follows. (i) From the cross-section formulas (3.17), (3.18), and (A1) through (A12) for $K\rightarrow L$ transitions, we may derive $L\rightarrow L$ and $L\rightarrow K$ cross sections by replacing the quantities m_{11}, m_{12}, m'_{12}, and m_{22} of Eq. (3.16) with the corresponding quantities calculated for the $2s_{1/2}$, $2p_{1/2}$, $2p_{3/2}$ final states and by inserting the appropriate terms (5.4) into

(3.16). While the integrals (5.4) are easily evaluated analytically, the complete cross-section calculation requires the evaluation of two-dimensional integrals. (ii) For the M shell and higher shells we use nonrelativistic electron wave functions, which amounts to setting $b_\kappa=0$ in (5.4b), thus considerably simplifying the calculation. Alternatively, one may directly use the nonrelativistic density matrix.[16] (iii) For initial M-shell states we have calculated P_h from (5.9), setting $\bar{b}_\kappa(\lambda)=0$, appropriate for nonrelativistic electron motion. In this case, new cross-section formulas were formulated. (iv) These formulas could then be used for all final states by merely modifying the quantities a_κ and b_κ in (5.4) and (3.16).

The use of nonrelativistic electron wave functions for higher shells disregards magnetic capture[11] via the Dirac magnetic moment of the electron. However, since this capture mechanism is important only at high values of γ, where the contribution of higher shells is much reduced, the neglect of magnetic capture for these shells does not appreciably affect the total cross sections.

B. The post and the prior form of the cross section

As mentioned at the beginning of Sec. III, the eikonal theory is asymmetric with respect to target and projectile. Depending on whether the electron-target or the electron-projectile interaction is treated nonperturbatively (i.e., approximately in all orders of perturbation theory) one obtains different results. This is referred to as the post-prior discrepancy, which is inherent in the eikonal approach as well as, e.g., in the strong-potential Born approximation.[20]

For definiteness, the formulation of Ref. 12 and that given above has been based on the prior version of the theory. The post version may be obtained immediately by interchanging target and projectile, i.e., $Z_p\to Z_t$, $Z_t\to Z_p$, $Z_t'\to Z_p'=Z_p$, and initial and final states. The initial and final states must be treated symmetrically in averaging or summing over both of them.

With the existence of two versions of the theory, the problem arises as to which one is appropriate for a given case. In principle, the answer is unique: The stronger of the two potentials Z_p/r_p or Z_t/r_t should be treated nonperturbatively and the other one in first order. Identifying the charge number Z_p or Z_t with the parameter that measures the strength of the potential customarily leads to the "higher-charge" prescription:

$$\begin{aligned}&\text{if } Z_p<Z_t \text{ then use the prior } (Z_t') \text{ form},\\ &\text{if } Z_t<Z_p \text{ then use the post } (Z_p') \text{ form}.\end{aligned}\tag{5}$$

Here the prime on Z_t' (Z_p') provides a signature that this quantity is retained in the eikonal phase to describe the distortion in the final (initial) channel. Prescription (5) does not take into account which electron-nucleus separations are most heavily weighted in the matrix element. This is justified if the initial and final principal quantum numbers, n_t and n_p, are the same, but if they are not, the two potentials are weighted at different electron-nucleus separations. In fact, since for hydrogenic systems,

$$\left\langle\frac{Z}{r}\right\rangle_n=\frac{Z^2}{n^2}\,,\tag{6}$$

irrespective of l and m, the parameter by which to measure the strength of a Coulomb potential should be Z/n rather than Z. This leads us to the following "higher-potential" prescription:

$$\begin{aligned}&\text{if } \frac{Z_p}{n_p}<\frac{Z_t}{n_t} \text{ then use the prior } (Z_t') \text{ form},\\ &\text{if } \frac{Z_t}{n_t}<\frac{Z_p}{n_p} \text{ then use the post } (Z_p') \text{ form}.\end{aligned}\tag{7}$$

We suggest that prescription (7) should be better for deciding which of the two potentials is the stronger one, and accordingly has to be treated nonperturbatively. Obviously, this prescription may lead to different choices for different combinations of initial and final shells. In Sec. IV we compare the predictions of both prescriptions, (5) and (7), with experimental data.

C. A simple scaling rule for transitions involving higher initial and final shells

For heavy-collision systems and not-too-high velocities, many principal shells in the target and in the projectile may contribute to the cross section. If this is the case, numerical calculations based on the exact formulation of the theory become rather lengthy, and it would be convenient to have a simpler formula suitable for realistic estimates.

In the special case of $1s_{1/2}-1s_{1/2}$ transitions, a simple closed formula has been derived[12] from an αZ expansion ($\alpha=\frac{1}{137}$). The results agree well with those derived from exact eikonal calculations[11] for all but the highest target and projectile charges. For reference we repeat the formula here[12]

$$\begin{aligned}\sigma^{\rm eik}_{1s-1s}&=\frac{2^8\pi Z_p^5Z_t^5}{5v^2(Z_t^2+p_-^2)^5}\frac{\gamma+1}{2\gamma^2}\frac{\pi\eta Z_t'}{\sinh(\pi\eta Z_t')}\exp[-2\eta Z_t'\tan^{-1}(-p_-/Z_t)](S_{\rm eik}+S_{\rm magn}+S_{\rm orb})\,,\\ S_{\rm eik}&=1+\frac{5}{4}\eta\frac{Z_t'}{Z_t}p_-+\frac{5}{12}\eta^2\frac{(Z_t')^2}{Z_t^2}p_-^2+\frac{1}{6}\eta^2(Z_t')^2\,,\\ S_{\rm magn}&=-\delta^2+\tfrac{5}{16}\delta^4+\tfrac{5}{8}\delta^2\frac{\gamma}{\gamma+1}\frac{Z_t'}{Z_t}+\tfrac{1}{4}\delta^2\eta^2(Z_t')^2+\tfrac{5}{48}\delta^4\eta^2(Z_t')^2\,,\end{aligned}\tag{8}$$

$$S_{\rm orb}=\frac{5\pi}{18}\delta\alpha(Z_p+Z_t)-\frac{5\pi}{36}\delta^3\alpha(Z_p+Z_t)-\tfrac{5}{8}\delta\alpha Z_t\eta Z_t'(1-\tfrac{1}{2}\delta^2)-\frac{5\pi}{18}\delta\frac{\gamma}{\gamma+1}\alpha Z_p\frac{Z_t'}{Z_t}$$
$$+\frac{5\pi}{28}\delta\left[\frac{\gamma}{\gamma+1}\right]^2\alpha Z_p\frac{(Z_t')^2}{Z_t^2}-\frac{5\pi}{28}\delta\frac{\gamma}{\gamma+1}\alpha(Z_p+Z_t-\delta^2Z_p)\frac{Z_t'}{Z_t}\ ,$$

$\eta=1/v$, $p_-=\eta(E_f/\gamma-E_i)$, E_i and E_f are relativistic atomic energies, $Z_t'=Z_t$ for the eikonal (and $Z_t'=0$ for the OBK) approximation, and $\delta=[(\gamma-1)/(\gamma+1)]^{1/2}$. The significance of the eikonal term $S_{\rm eik}$, the magnetic term $S_{\rm magn}$, and the orbital term $S_{\rm orb}$ has been discussed in detail in Ref. 12.

For higher principal shells, the cross sections in the nonrelativistic OBK scale with Z/n,[21] and this holds also[16] in the prior (post) form of the eikonal approximation for the final (initial) state. In the following, we show that eikonal cross sections *averaged over a complete principal shell* approximately scale with Z/n for initial and final states. Let

$$[\mathcal{F}\{\phi(\mathbf{r})\}]_{\mathbf{q}}=(2\pi)^{-3/2}\int\phi(\mathbf{r})e^{i\mathbf{q}\cdot\mathbf{r}}d^3\mathbf{r} \tag{9}$$

denote the Fourier transform of some function $\phi(\mathbf{r})$ and $\phi_{nlm}(Z,\mathbf{r})$ a hydrogenic wave function associated with the charge Z. Then, the *diagonal* part of the density matrix in momentum space (which enters in the eikonal cross section) can be shown to be equal to[16,22]

$$\Phi_n(Z,q)=\frac{1}{n^2}\sum_{l,m}|[\mathcal{F}\{\phi_{nlm}(Z,\mathbf{r})\}]_{\mathbf{q}}|^2$$
$$=\frac{8q_n^5}{\pi^2(q^2+q_n^2)^4}\ , \tag{10}$$

where $q_n=Z/n$. Obviously, expression (10) depends on Z and n only through the combination Z/n. Now, with the aid of the Schrödinger equation, we obtain another density matrix in momentum space,[16]

$$G_n(Z,q)=\frac{1}{n^2}\sum_{l,m}|[\mathcal{F}\{(Z/r)\phi_{nlm}(Z,\mathbf{r})\}]_{\mathbf{q}}|^2$$
$$=\frac{2q_n^5}{\pi^2(q^2+q_n^2)^2}\ , \tag{11}$$

which again depends only on the quantity Z/n.

In the OBK approximation, the capture cross section[21] from an averaged initial state n_t to an averaged final state n_p is a simple momentum integral over $\Phi_n(Z_t,q)G_n(Z_p,q)$ and hence depends only on Z_p/n_p and Z_t/n_t.

In the prior form of the eikonal approximation, the transition amplitude between the time-dependent atomic states $\Psi(t)$ (including translation factors) can be expanded[17] as

$$A_E=-i\int_{-\infty}^{\infty}dt_1\left\langle\Psi_{n_pl_pm_p}(t_1)\left|\frac{Z_p}{r_p(t_1)}\right|\Psi_{n_tl_tm_t}(t_1)\right\rangle$$
$$+(-i)^2\int_{-\infty}^{\infty}dt_1\int_{t_1}^{\infty}dt_2\left\langle\Psi_{n_pl_pm_p}(t_1)\left|\frac{Z_t}{r_t(t_2)}\frac{Z_p}{r_p(t_1)}\right|\Psi_{n_tl_tm_t}(t_1)\right\rangle+\cdots\ . \tag{12}$$

If we include in A_E terms only up to second order in the potentials Z_p/r_p and Z_t/r_t, we immediately realize that only terms of the structure (10) and (11) and mixed terms involving $\mathrm{Re}[\mathcal{F}^*\{(Z/r)\phi\}\mathcal{F}\{\phi\}]$ enter into the cross section. All of these terms scale with Z_p/n_p and Z_t/n_t. Therefore, up to second order in the potentials, the nonrelativistic eikonal approximation cross sections for $Z_p,n_p\rightarrow Z_t,n_t$ transitions scale as the $1s$-$1s$ one for $Z_p/n_p\rightarrow Z_t/n_t$. Also, it has been shown that for high velocities, only single and double scattering terms contribute significantly to the cross section.[18] One may conclude that nonrelativistic, and approximately relativistic, eikonal cross sections scale to a good approximation with Z_p/n_p and Z_t/n_t. Therefore, we propose the following scaling rule: *Approximate relativistic capture cross sections averaged over initial and final orbital states for arbitrary initial and final principal shells can be obtained from formula (8) for relativistic 1s-1s cross sections*[12] *by replacing* Z_p *with* Z_p/n_p *and* $Z_t=Z_t'$ *with* Z_t/n_t *in the prior form. To obtain the post form, the target and projectile charges and the initial and final states are interchanged.*

It should be noted that if this scaling rule is adopted, the decision between the prior and the post form will be automatically based on criterion (7). In Sec. IV we compare the results derived from the scaling rule with those of exact eikonal calculations and with experimental data.

D. Radiative electron capture

The cross section for the radiative capture of an electron into the projectile shell n_p can be calculated from the

cross section for the photoelectric absorption of a photon with energy $k=\gamma-1+E_i(n_p)/mc^2$ using[23]

$$\sigma_{\mathrm{REC}}(n_p)=Z_t\left[\frac{k}{\beta\gamma}\right]^2\sigma_{\mathrm{PE}}(n_p,k)\ . \tag{13}$$

(If the subshells have different binding energies, one must sum over subshell photoelectric cross sections.) Most calculations of photoelectric cross sections are for neutral atoms. However, needed in Eq. (13) is the cross section for the removal of an electron from a one- or two-electron atom. Research on the photoeffect has evolved from calculations using nonrelativistic one-electron wave functions, to calculations using Dirac wave functions, and finally tables of photoelectric cross sections calculated using Hartree-Fock-Slater wave functions have been published.[24,25] It has been found that for the relevant photon energies, the ratio of the many-electron to Dirac photoelectric cross sections is approximately equal to the ratio of the bound-state electron density at the origin, calculated using many-electron wave functions to that calculated using Dirac wave functions.[26] Therefore, in the present cases, we divided the many-electron photoelectric cross sections by the bound-state normalization factors, 0.96 for the K, 0.81 for the L, and 0.43 for the M shells of Xe, to obtain Dirac-like photoelectric cross sections.[27]

IV. RESULTS

A. Higher-shell contributions

Figure 4 shows calculated contributions from various transitions in 1050-MeV/amu Ne + Ag, 197-MeV/amu Xe + Ag, and 82-MeV/amu Xe + Au collisions. In these

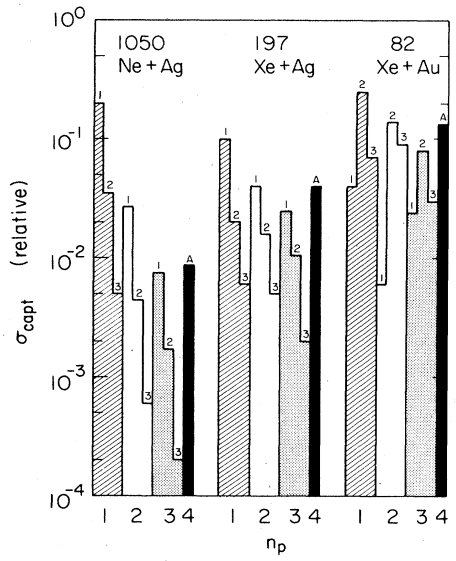

FIG. 4. Relative cross sections for the capture of electrons from target shells with $n_t=1,2,3$ (A is the sum of all target shells) into bare projectile shells with $n_p=1,2,3$, and all shells with $n_p\geq 4$ for 1050-MeV/amu Ne + Ag, 197-MeV/amu Xe + Ag, and 82-MeV/amu Xe + Au. The numbers above each bar are target principal quantum numbers n_t, and on the abscissa are n_p numbers.

calculations, the higher-potential post-prior criterion, Eq. (7), has been used. The capture cross sections are for bare projectiles colliding with completely occupied target atoms. For the projectile, the full nuclear charge was used, but for the target atoms, we used effective nuclear charges based on the Slater rules[28]

$$Z_t(n)\rightarrow Z_t^*=Z_t-\Delta Z(n)\ , \tag{14}$$

where $\Delta Z=0.3$ for the K shell, 4.15 for the L shell, 11 for the $3s$ and $3p$ shells, and 21 for the $3d$ shell. Unlike in Ref. 11, experimental electron binding energies were not used. The initial and final energies are given by

$$\begin{aligned} &E_{i,f}=c^2[1-\alpha^2Z^2(1)]^{1/2} \text{ for the } K \text{ shell}\ , \\ &E_{i,f}=c^2[1-\tfrac{1}{2}\alpha^2Z^2(n)n^{-2}] \text{ for } n>1\ , \end{aligned} \tag{15}$$

where $\alpha=1/137.036$. To save computation time, we used nonrelativistic L and M target and projectile wave functions. The equations for L are, therefore, obtained from Eqs. (A1)—(A12) of Ref. 12 by taking the nonrelativistic limit of the wave functions. It was found that even for Xe + U collisions, one obtains nearly identical results using relativistic and nonrelativistic L orbitals. For the final state, we included all projectile states with $4\leq n_p\leq 10$, by summing the Fock distribution, Eq. (10), and assuming that the final-state energy is independent of n and equal to the $n=4$ one for $n>4$. Since $E_f(n)$ is close to c^2 for $n>4$, this approximation should have only a small effect on the capture cross sections.

For hydrogenic projectile and target wave functions, and for NRC at high velocities, the cross sections should vary as

$$\sigma(n_p,n_t)\sim\left[\frac{Z_p}{n_p}\right]^3\left[\frac{Z_t^*}{n_t}\right]^3 Z_p^2(Z_t^*)^2\ . \tag{16}$$

This situation is nearly realized in Ne + Ag collisions, as shown in Fig. 4. The cross sections for fixed n_t fall off as n_p^{-3}, but the cross sections for fixed n_p fall off faster with n_t since $Z_t^*(n)$ decreases with n_t [Eq. (14)]. The cross section for all projectile states with $n_p\geq 4$ from all K, L, and M target orbitals is nearly equal to the total $n_p=3$ cross section. Since Slater screening reduces the effective charge for $n_t\geq 4$ to negligible values, it is unnecessary to include target states with $n_t\geq 4$.

In 197-MeV/amu Xe + Ag collisions, the relative contributions from higher shells is greater than for Ne + Ag collisions. This difference occurs because the momentum transfer $|p_-|$ for target L to projectile K capture is significantly smaller than for K to K capture. Since the cross sections in Eq. (8) vary as p_-^{-10} (if $p_-^2\gg Z_p^2$), the n^{-3} scaling, Eq. (16), is no longer valid. The scaling breaks down completely in 82-MeV/amu Xe + Au collisions where target L-electron capture is dominant, and capture into almost any shell of the projectile, $n_p=1,2,3$, and the sum for $n_p\geq 4$, is of the same order of magnitude. Clearly any theory of electron capture that includes only K-K electron transfer will grossly underestimate the total cross sections in this regime.

B. Comparison with experiment

Measurements of single-electron capture were made using Xe^{52+}, Xe^{53+}, and Xe^{54+} ions. The results depend on two summed cross sections,

$$\sigma_K = \sum_{n_t=1}^{3} \sigma_{\mathrm{NRC}}(1,n_t) + \sigma_{\mathrm{REC}}(1) ,$$

and

$$\sigma_H = \sum_{n_p=2}^{10} \sum_{n_t=1}^{3} \sigma_{\mathrm{NRC}}(n_p,n_t) + \sigma_{\mathrm{REC}}(n_p) , \tag{17}$$

where $\sigma_{\mathrm{NRC}}(n_p,n_t)$ is the NRC cross section from the target shell n_t into the projectile shell with n_p, and $\sigma_{\mathrm{REC}}(n_p)$ is the REC cross section [all target shells are automatically summed over by including the factor of Z_t in Eq. (13)]. The measured attachment cross sections for Xe^{54+}, Xe^{53+}, and Xe^{52+} are given by

$$a_0 = \sigma_K + \sigma_H ,$$
$$a_1 = \tfrac{1}{2}\sigma_K + \sigma_H , \tag{18}$$

and

$$a_2 = \sigma_H ,$$

respectively.

Attachment cross sections for Xe^{52+} and Xe^{54+} ions are shown in Figs. 5 and 6. For low Z_t, REC dominates and the present measurements are in good agreement with theory. For high Z_t, the total cross sections were calculated using both the higher charge, Eq. (5), and the higher potential, Eq. (7), prescriptions for taking either the post or prior form. In general, for high Z_t, the higher-potential prescription agrees better with the data, but for $Z_p \approx Z_t$, the higher-charge prescription agrees better.

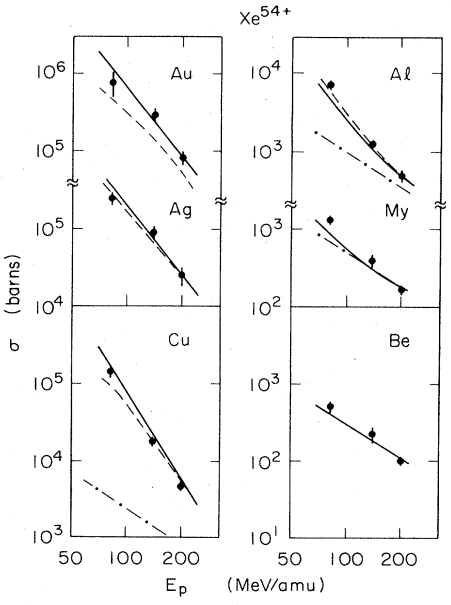

FIG. 5. Electron-attachment cross sections for Xe^{54+} ions incident on Be, Mylar (My), Al, Cu, Ag, and Au targets. The solid line gives the total REC and NRC cross sections where the NRC cross sections were calculated with the eikonal approximation according to the higher potential post-prior prescription, Eq. (7). For the dashed lines, the higher-charge criterion, Eq. (5), was used. The chain curve shows the separate REC cross section which is dominant in Xe + Be collisions.

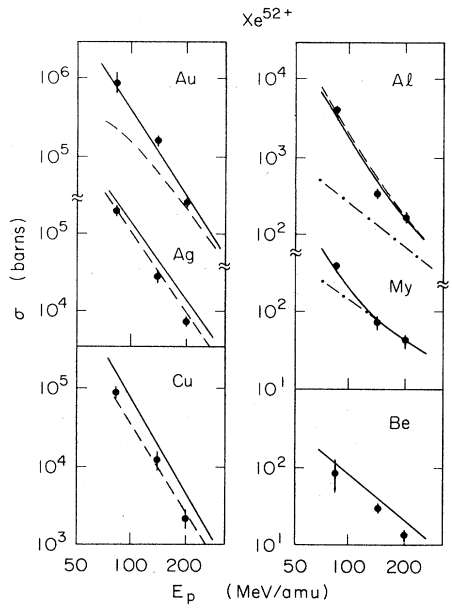

FIG. 6. Same as Fig. 5 for Xe^{52+} ions, where capture into Xe K shell is not allowed, hence only capture into the L, M, and higher orbitals of Xe occurs.

Figures 7–9 compare measured cross sections with scaling-law calculations for NRC cross sections. Identical REC cross sections and identical Slater screened-target charges were used as in Figs. 5 and 6. (However, the $3d$ charge is not used in the scaling-law calculations since the formula is for the sum over all $n=3$ subshells.) For 1050-MeV/amu Ne collisions, it was found that increasing Z_t' in the first line in Eq. (8) by a factor of 1.16 brought the L-capture cross sections into better agreement with numerical calculations. We have employed this factor for all shells except for $1s$-$1s$ transitions. Although the scaling law is justifiable by the arguments in Sec. III C, this factor is not. Without it, the calculated cross sections are too high by factors of 1.5 to 2. For the purpose of estimating NRC cross sections with a simple formula, the use of this *ad hoc* factor is recommended. It gives good results not only for Xe collisions, as shown in Figs. 7 and 8, but for many other cases including low-Z projectiles, as shown in Fig. 9.

In comparing measured cross sections with calculations that include capture into projectile states with $n_p \geqq 4$, one should consider possible reionization of the captured electron before the ion leaves the target. In the worst case, assuming the electron does not decay to the ground state, the resulting cross section for $n=4$ capture would be given by

$$\sigma(4) = \sum_{n_t} \sigma(4,n_t)(1 - s_4 T/2) , \tag{19}$$

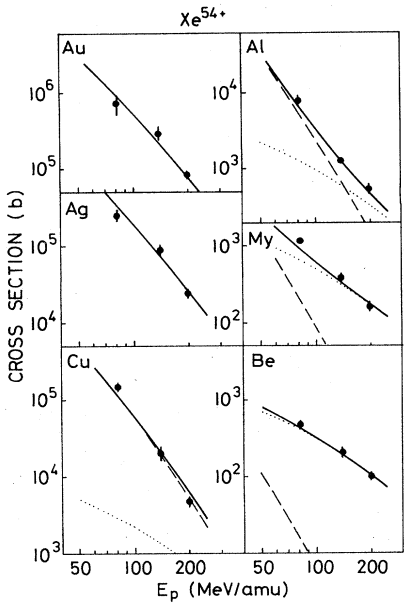

FIG. 7. Electron-attachment cross sections for Xe^{54+} ions. The dotted line shows the REC cross section, the dashed line the NRC cross section calculated using the scaling-law formula, and the solid line shows the total-capture cross section.

where s_4 is the $n_p=4$ ionization cross section. This can be a potential problem for collisions at low velocities and with low-Z projectiles where the outer-shell ionization cross sections are enormous and the decay cross sections are small. We have verified that for the present Xe ions, the worst-case (no decay) correction to the capture cross sections is much smaller than the experimental uncertainties.

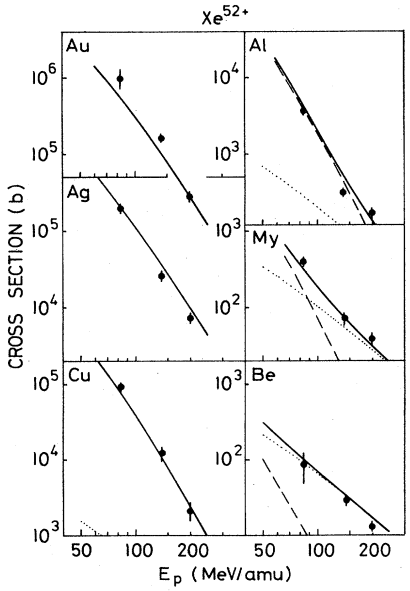

FIG. 8. Same as Fig. 7 for Xe^{52+} ions, where capture into the Xe K shell is not allowed.

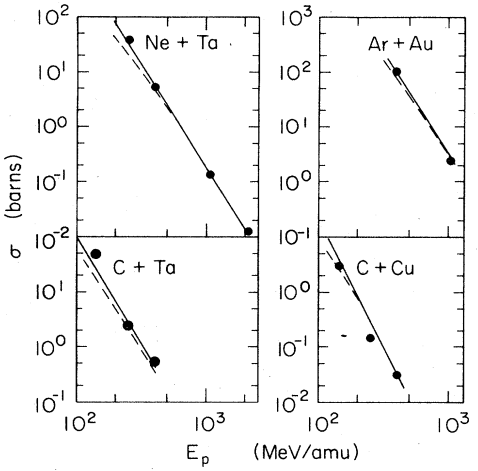

FIG. 9. Nonradiative electron-attachment cross sections for low-Z projectiles calculated using the scaling law (solid line) and the numerical eikonal formulas with prescription (7) (dashed line).

C. Multielectron capture

For 82-MeV/amu Xe ions, the cross sections for double and triple electron capture are large compared to the single-electron-capture cross sections at high Z_t, as shown for the Xe^{54+} ions in Fig. 10. The starting point in the analysis of double-electron capture is the independent-electron approximation.[29] If $P_0(b)$ is the single-electron capture probability in a collision with impact parameter b for zero-electron Xe^{54+} ions, and $P_1(b)$ is that for capture into Xe^{53+} ions, the cross section for double-electron capture into Xe^{54+} is given by

$$\sigma_D = \int_0^\infty db\, 2\pi b P_0(b) P_1(b) \ . \tag{20}$$

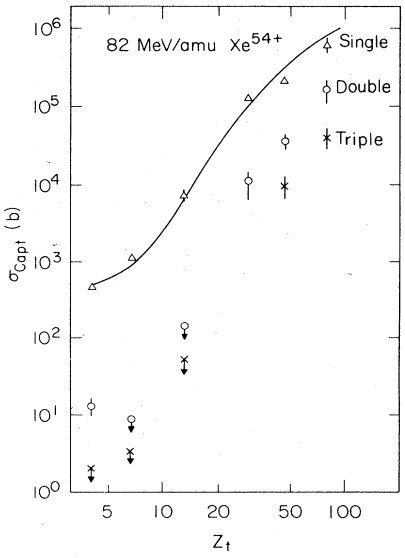

FIG. 10. Single- double-, and triple-electron attachment to 82-MeV/amu Xe^{54+} projectiles incident on various target atoms from Be to U. The curve was calculated using the scaling law.

Equation (20) can be viewed as taking a weighted average of the probability P_1 over the range of impact parameters contributing to electron capture. To obtain a large double-capture cross section, the probability P_1 (or P_0) should be large at the impact parameters contributing most to the total cross section. This requires a large capture cross section, and that the probability should fall off rapidly with b. The REC cross section is never very large and impact parameters as large as the target atomic radius contribute, so double REC is negligible (see the Appendix). For 82-MeV/amu Xe + Au collisions, the NRC cross sections are large ($>10^6$ barns), and the relatively large values of the momentum transfer imply that the probability falls off sufficiently steeply with impact parameter so that large NRC probabilities can be expected. As the present eikonal cross-section evaluations did not calculate the impact-parameter dependence, we cannot calculate the double-capture cross section for NRC, but the present considerations imply that double capture may be understandable in the independent-electron approximation.

V. CONCLUSIONS

Our measurements of electron capture by highly-stripped relativistic Xe ions show that NRC into excited states of the projectile dominates over ground-state capture at high target atomic numbers. To account for excited-state capture, eikonal approximation calculations that include all projectile states up to $n=10$ and all target K, L, and M orbitals have been made. The eikonal calculations are in reasonable agreement with measurements.

We emphasize that the eikonal approximation handles the electron-nucleus interaction of one (usually the higher) atomic charge to all orders of perturbation theory and the other interaction to first order. The eikonal approximation is less valid, therefore, for near-symmetric collisions where both interactions should be treated in higher order. The imposition of this asymmetric theory on near-symmetric collisions leads to differences between cross sections calculated in the post versus prior form. By taking into account the spatial extension of the electron shells involved, the present paper proposes a new criterion, Eq. (7), for choosing the post or prior form, and most of the data seems to be in accord with the resulting choice. However, in a few cases the data are better represented by the conventional choice, Eq. (5). This may reflect the fact that criterion (7), being based on a diagonal matrix element, tends to overestimate the effect of the shell size.

The eikonal approximation is a high-velocity approximation. For low-Z ions, we noted in Ref. 11 that the calculations give lower cross sections than experiment when the ion velocity is less than $\sim 2Z_t$. However, in those cases K-K transfer is dominant (Fig. 4). When outer-shell transitions are dominant, the effective limiting Z is smaller. Therefore, although we saw large discrepancies for 140-MeV/amu C + Au collisions where K to K capture is dominant, we see smaller ones in lower-velocity 82-MeV/amu Xe + Au collisions where outer-shell capture is dominant.

ACKNOWLEDGMENTS

This work was supported in part by National Science Foundation Grant No. PHY-83-13676 (Stanford University), by SRI-International (J.E.), by the Director, Office of Energy Research, Division of Nuclear Physics of the Office of High Energy and Nuclear Physics of the U.S. Department of Energy under Contract No. DE-AC03-76SF00098 (Lawrence Berkeley Laboratory), and by the U.S. Department of Energy under Contract No. DE-AC02-76CH00016 (Brookhaven National Laboratory). We thank the Bevalac operators and staff for their skill and persistence in the delivery of 21 different beams in 76 hours.

APPENDIX: DOUBLE RADIATIVE ELECTRON CAPTURE (DREC)

The probability P_0 for REC is given by[30]

$$P_0(b)=\sigma_{\mathrm{REC}}(Z_t=1)\int_{-\infty}^{\infty} dz\,\rho(R)\ , \tag{A1}$$

where $\rho(R)$ is the target electron density and $R^2=b^2+z^2$. Since the electron density is normalized so that

$$\int_0^{\infty} db\,2\pi b\int_{-\infty}^{\infty} dz\,\rho(R)=Z_t\ , \tag{A2}$$

one automatically obtains the correct total REC cross section into all projectile shells, $Z_t\sigma_{\mathrm{REC}}(Z_t=1)$. One can calculate the atomic density with the Thomas-Fermi theory.[31] A numerical evaluation of the double-capture cross section yields

$$\sigma_{\mathrm{DREC}}=A\sigma_{\mathrm{REC}}^2(Z_t)a_0^{-2}\ , \tag{A3}$$

where $A\sim 0.13Z_t^{1/2}$, independent of the projectile charge or energy. Since σ_{REC} is much smaller than a_0^{-2}, this leads to negligibly small double-REC cross sections, 0.0016 b for 82-MeV/amu Xe^{54+} + Be and 3.8 b for Xe^{54+} + U. On this basis, the measured double-capture cross section shown in Fig. 10 of ~ 10 b for 82-MeV/amu Xe^{54+} + Be where REC is dominant cannot be understood.

---

*On leave from Bereich Kern- und Strahlenphysik, Hahn-Meitner Institut für Kernforschung Berlin, D-1000 Berlin 39, Federal Republic of Germany and Fachbereich Physik, Freie Universität Berlin, D-1000 Berlin 39, Federal Republic of Germany.

[1]R. Anholt, Phys. Rev. A **31**, 3579 (1985).

[2]H. Crawford, Ph.D. thesis, University of California, 1979 [Lawrence Berkeley Laboratory Report No. LBL-8807 (unpublished)].

[3]H. Gould, D. Greiner, P. Lindstrom, T. J. M. Symons, and H. Crawford, Phys. Rev. Lett. **52**, 180 (1984); **52**, 1654(E) (1984).

[4]P. Thieberger, H. E. Wegner, J. Alonso, H. Gould, R. Anholt,

and W. E. Meyerhof, in Proceedings of the 1985 Particle-Accelerator Conference, Vancouver, British Columbia [IEEE Trans. Nucl. Sci. **32**, 1767 (1985)].
[5]H. D. Betz, Rev. Mod. Phys. **44**, 465 (1972).
[6]R. Shakeshaft, Phys. Rev. A **20**, 779 (1979).
[7]B. L. Moiseiwitsch and S. G. Stockman, J. Phys. B **13**, 2975 (1980).
[8]R. M. Drisko, Ph.D. thesis, Carnegie Institute of Technology, 1955.
[9]W. J. Humphries and B. L. Moiseiwitsch, J. Phys. B **17**, 2655 (1984).
[10]W. J. Humphries and B. L. Moiseiwitsch, J. Phys. B **18**, 2295 (1985).
[11]R. Anholt and J. Eichler, Phys. Rev. A **31**, 3505 (1985).
[12]J. Eichler, Phys. Rev. A **32**, 112 (1985).
[13]D. E. Greiner, P. J. Lindstrom, F. S. Bieser, and H. H. Heckmann, Nucl. Instrum. Methods **116**, 21 (1974).
[14]V. S. Nikolaev, Usp. Fiz. Nauk **85**, 679 (1985) [Sov. Phys.—Usp. **8**, 269 (1965)].
[15]S. Datz, H. O. Lutz, L. B. Bridwell, C. D. Moak, H. D. Betz, and L. D. Ellsworth, Phys. Rev. A **2**, 430 (1970).
[16]F. T. Chan and J. Eichler, Phys. Rev. Lett. **42**, 58 (1979); J. Eichler and F. T. Chan, Phys. Rev. A **20**, 104 (1979).
[17]J. Eichler and H. Narumi, Z. Phys. A **295**, 209 (1980).
[18]L. J. Dubé and J. Eichler, J. Phys. B **18**, 2467 (1985).
[19]D. P. Dewangen and J. Eichler, J. Phys. B **18**, L65 (1985).
[20]J. Macek and S. Alston, Phys. Rev. A **26**, 250 (1982).
[21]M. R. C. McDowell and J. P. Coleman, *Introduction to Ion-Atom Collisions* (North-Holland, Amsterdam, 1970).
[22]V. Fock, Z. Phys. **98**, 145 (1935).
[23]V. B. Berestetskii, E. M. Lifshitz, and L. P. P. Pitaevskii, *Relativistic Quantum Theory, Part 1* (Pergamon, Oxford, 1971).
[24]R. H. Pratt, A. Ron, and H. K. Tseng, Rev. Mod. Phys. **45**, 273 (1973).
[25]J. H. Scofield, University of California Report No. UCRL-51326, 1973 (unpublished).
[26]R. H. Pratt, Phys. Rev. **119**, 1619 (1960).
[27]R. D. Schmickley, Ph.D. thesis, Stanford University, 1966.
[28]J. C. Slater, Phys. Rev. **36**, 57 (1930).
[29]J. H. McGuire and L. Weaver, Phys. Rev. A **16**, 41 (1977).
[30]R. Shakeshaft and L. Spruch, Rev. Mod. Phys. **51**, 369 (1979).
[31]P. Gombas, *Statistische Theorie des Atoms* (Springer, Wien, 1949).